Presented at American Institute of
Metallurgical Engineering Spring
Meeting, Las Vegas, Nevada,
May 11-14, 1970

UCRL-19648
Preprint

Conf-700553--1

ELECTRON MICROSCOPY INVESTIGATIONS OF FERROUS MARTENSITES

Gareth Thomas

January 1971

AEC Contract No. W-7405-eng-48

LAWRENCE RADIATION LABORATORY
UNIVERSITY of CALIFORNIA BERKELEY

UCRL-19648

DISCLAIMER

ELECTRON MICROSCOPY INVESTIGATIONS OF FERROUS MARTENSITES

Gareth Thomas
Department of Materials Science and Engineering
University of California, Berkeley, California 94720

ABSTRACT

This paper is concerned with electron metallography of bcc or bct ferrous martensite in which particular attention is paid to the characterization of substructures. The transformation substructure is complex and new results are reported on multiple {112} twinning. The factors controlling the martensitic substructure are evaluated and it is concluded that the strength and deformation characteristics of martensite are the most important in determining whether the transformation deformation occurs by slip or twinning (or both).

An appraisal is given of in situ transformations in the electron microscope particularly with regard to the nucleation problem and investigations of the interfacial structures. The potential role of high voltage electron microscopy is also discussed and some recommendations are offered for future investigations.

1. Introduction

The first results of transmission electron microscopy studies of foils made from carbon and alloy martensitic steels were published just over ten years ago.[1-3] Since then numerous papers have appeared which deal largely with characterizing particular steels, and relatively few attempts have been made to investigate quantitatively the problems associated with martensite nucleation, the nature of the austenite-martensite interface, and the orientation relationships and substructural characteristics of individual transformation events. Considerable work has been done on the relationship between submicrostructure and properties of steels, and recently systematic efforts have been directed at understanding the role of alloying elements in these relations. Some recent review papers which contain electron microscopy data include those of Wayman[4] Magee[5] and Nutting.[6] Reviews of electron microscopy applications to investigations of phase transformations in general include those of Thomas[7-9] and Hirsch et al.[10] These publications describe in detail the important experimental and theoretical factors involved in the use of electron microscopy and diffraction.

The present paper is concerned with electron metallography of ferrous martensites, particularly transformation substructures. Some discussion is also presented of nucleation and other aspects of the transformation. No discussion will be given of martensite other than bcc or bct (i.e. epsilon [hcp] martensite is excluded) nor of strain induced martensite.

It is hoped that some of the ideas presented here and the commentaries on both advantages and disadvantages of electron microscopy may be useful in future investigations.

2. Martensite Nucleation and Transformations in Foils

The electron microscope provides information on morphology, crystallography and composition. The analyses are usually carried out on foils prepared from bulk transformed specimens, but dynamic experiments inside the microscope can also be done directly on foils.[9] However, even at 500-1000 kV foils must be 2μ thick or less[11,12] for electron transmission and this is of the same order of magnitude as the dimensions of single martensite crystals. Thus, in foils, the transformation conditions are essentially two-dimensional in nature and are quite different from those involved in bulk transformations. Consequently the crystallography and substructure may then also be quite different. These problems were first demonstrated by Pitsch[3] who studied the martensite transformation directly in several ferrous alloys.

Except for the first direct observations of the FCC-HCP transformation in cobalt[13] and that of heterogeneous nucleation of γ' in Al-Ag[14] and surface precipitation in Al-4% Cu[15] in the electron microscope, there are as yet no other direct observations of nucleation processes. In the simple FCC⇄HCP systems, theory predicts specifically defined imperfections for the nucleation site, viz. dislocations and stacking faults, and it is possible to identify and so locate the nucleation site prior to the transformation process. As a result it has been possible to follow in detail both nucleation and growth events and the theory of heterogeneous nucleation for these transformations has been confirmed. As far as FCC → BCC or BCT martensites are concerned, the nucleation theory is not at present very satisfactory. There is no clear evidence for nucleation sites except for the case of strain induced martensites where intersecting epsilon

martensite and slip bands, and twin boundaries have all been observed to give rise to α martensite crystals.[16,17] Magee[5] has emphasized the importance of twin boundary sites, heterogeneous nucleation in general, and autocatalysis.

Figure 1 indicates that dislocations and stacking faults may have caused the formation of the martensite in the Fe/8Cr/1C alloy. It is also possible that these defects are a consequence of the formation of martensite. Direct observations of transformation in this system are planned and should help to distinguish between these possibilities.

The present thermodynamic theory requires the existence of "embryos." Pati and Cohen[18] calculated the probability of observing embryos as 2 in 10^5. Warlimont[19] interprets this probability in terms of the necessity of examining an area ~ $20cm^2$ in order to find one nucleus of the most effective size and structure. Although these are almost impossibly small probabilities, the fact remains that martensitic reactions do occur in thin foils, probably as a result of strain induced or autocatalytic events or because constraints may be removed on thinning.

As far as direct observations of the transformation are concerned, several important factors must be considered. For example:

1. It is essential to have a goniometric specimen (double-tilt or tilt-rotation) holder so that contrast experiments and diffraction data can be obtained at all temperatures. The heating-cooling response of the stage must be adequate to permit transformation to occur and contamination must be avoided (see ref.21).
2. The area being examined suffers some beam heating and consequently as the Ms temperature is approached the transformation will

take place outside the area being examined.[21] In all experiments to date nucleation events must have occurred outside the field of view.

3. Because the transformation occurs very rapidly, it is impossible to study both the morphology (i.e. the image) and the crystallography (diffraction pattern) during the transformation. It is helpful, therefore, to use single crystals of known orientation, for which the bulk crystallography is already documented. In most situations it is necessary to repeat experiments, studying one particular feature at a time. It will also be necessary to use high speed, high resolution movie techniques to record the transformation.

4. It is difficult, if not impossible, to mount a foil in the specimen holder without introducing some strains. The strained areas may then become preferential nucleation sites.

5. Some idea of when a transformation is occurring can be obtained by careful observance of the temperature rise associated with the release of the driving force. Our observations show a temperature rise of +30°C for Fe/24Ni/4Mo/0.28C and +60°C for Fe/25Ni/0.3V/0.3C during cold stage experiments on the martensitic transformation in foils of these steels.

6. Because of elastic relaxation, the macroscopic shape change in foils may not require the amount of lattice invariant shear (slip or twinning required by the phenomenological theories) necessary in bulk samples. Direct observations of martensite formation and growth will enable enalysis to be made of the origin of the martensite substructure, i.e. contributions from transformation deformation and subsequent accommodation deformation

may be distinguished by comparing foils of bulk transformed steel and transformed foils (Sec. 3).

7. It is not yet clear that the transformation in foils is always different from that in bulk, i.e. differing in crystallography and morphology. There is simply not enough data from bulk and foil specimens in the same alloys.

8. An important factor in the transformation of foils is the apparent change in Ms temperature with specimen thickness and cooling rate, e.g. due to precipitation or carbon segregation in austenite. The upper temperature limit of Ms has been observed to decrease when the specimen thickness is less than about 1μ.[19]

Warlimont[19] has recently studied the functional Ms dependence of thickness in Fe/Ni alloys. He found two opposing effects which produced a scattering of Ms to lower as well as to higher temperatures. He explained these results in terms of the distribution of nuclei per unit volume and to the effects of image forces on martensite nuclei (assuming heterogeneous nucleation). On the basis of the embryo theory, supposing there are 10^7 embryos/cc at the first nucleation stage,[18] then for a foil of volume 10^{-7} cm^3 (1000Å thick, x 1mm x 1mm) probably only one embryo would be present. Due to the greater penetration at high voltages a foil of 2μ thick should be transparent and in this case the number of embryos increases to 20. The work of Easterling and Swann[22] showed that small austenite particles in copper did not transform to martensite except after elastic deformation even though the bulk Ms is 600°C. Kinsman[23] showed, however, that if constraints are removed, e.g. by polishing the surrounding copper away, the austenite then transforms spontaneously.

Finally it is worth emphasizing that more attention should be paid to electron diffraction. Although electron diffraction patterns are widely used for orientation determinations, no attempts seem to have been made to investigate diffraction patterns before and during the $\gamma - \alpha$ transformation. Such work would be facilitated by using single crystals of appropriate orientation. Examination of the diffraction patterns, particularly the diffuse reflections, could provide information such as 1) what happens to the austenite at the transformation start, 2) the structure of the first formed martensite, 3) the shape of the first formed crystal. Double diffraction effects must be accounted for.[9,10]

3. Substructure of Martensite

1. General Morphology

There are two general morphologies of ferrous martensties, viz. dislocated laths and twinned plates. The dislocated laths are composed of elongated bundles of slightly misoriented subgrains, within which the dislocation density may vary with composition and cooling rate (specimen thickness) and is associated with the $\{111\}_\gamma$ habit.[2] An example is shown in Fig. 2. The laths can also be twin related. In low carbon steels adjacent laths appear to adopt different variants of the K-S orientation relationship.[61] The dislocation structure is very complicated and similar to that in α-Fe and metals of high stacking fault energy[24] after high speed deformation. Plate martensites contain fine transformation twins. Those within which the twin density varies and in which the twins do not extend completely across the plates

are associated with $\{225\}_\gamma$, $\{259\}_\gamma$ habits, whereas fully twinned plates correspond to the $\{3, 10, 15\}_\gamma$ habit. A summary including recent, as yet unpublished data is given in Table 1, and examples of these twinned structures are shown in Figs. 1, 3-6, 9, 11. In all cases the substructure within a given martensite grain is complex and in many fully martensitic steels the microstructures are often complex mixtures of dislocated and twinned martensites (Fig. 6) so that detailed microstructural analyses are very difficult to carry out.

The martensitic substructures may arise from two factors: 1) the lattice invariant shear of the transformation strain itself and this may be slip, twinning or a combination of both, and 2) plastic deformation of the martensite <u>after</u> its formation, due to accommodations resulting from the constraints of the surroundings. It follows that surface martensite or martensite formed in the thin foils should be less deformed than bulk martensite because of the absence of bulk constraints at the free surface. Unless the development of the substructure can be observed directly during the transformation (see Figs. 7, 8) it is not possible to distinguish between transformation and deformation substructures. This distinction is important in regard to relating observed structures to the shears proposed in the crystallographic theories.

At the present time there is agreement between the phenomenological theory and substructure only for the case of the $\{3, 10, 15\}_\gamma$ habits and $\{112\}\langle 11\bar{1}\rangle_\alpha$ twinning.[4] The $\{225\}_\gamma$ partially twinned martensites are very complex as will be shown in more detail in Section 3.2. Physically, of course, since the twinning dislocation must remain in the habit plane, and if the twin dislocation is of the $\bar{a}/6\langle 111\rangle$ type, then for cubic alloys

TABLE I

STRUCTURE OF BODY CENTERED FERROUS MARTENSITES FORMED ON COOLING THROUGH M_s-M_f*

Alloy System	Ms	Substructure/Composition**	Reference
Fe-C	>350°C	C < 0.3 mainly dislocated laths	1, 2, 28 40,
	<250°C	C > 0.6 mainly twinned plates	
Fe-Ni	>-50°C	Ni < 25 dislocated laths	1, 2, 39, 41, 42, 43
	-30°-150°C and below	Ni $\geq$ 30 mid-rib twinned only	44, 45, 48, 53
		Extent of twinning increases with % Ni, and lower M_s	
Fe-Ni-C	as above	Increase in carbon for same nickel content & vice-versa enhances twinning	1, 2, 40, 43 28, 48, 39, 61
Fe/25Ni/0.3C/4.5Mo	<-77°C	All mainly twinned. However	29, 30
+4.7 Cr	-16°C	ausforming causes precipitation	
+1.85V	-3°C	of carbides, so that the result-	
		ing martensite is less twinned.	
Fe-Ni-Co-C (1/2Mo/1/2Cr)	-260°C	C < 0.3 dislocated laths	31
	150-260°C	C > 0.4 twinned cobalt does not decrease twinning	
Fe-Ni-Co	as above		69
Fe/Cr/C	350-400°C	Partially twinned	
		Cobalt raises Ms - does not decrease % twinning	35
Fe-5Cr		dislocated laths	43

* All data here refer to nominal cooling rates. The Ms temperature and structure can be varied by varying quench rate (see text).

** Composition refer to weight %.

Alloy System	Ms	Substructure/Composition	Reference
Fe-8Cr-1C	-30°C	twin density decreases with increasing plate size	20, 25
Fe/5Ni/0.25C	315°C	mainly dislocated	36
Fe/3Mn/0.25C	315°C	mainly dislocated	36, 47
Fe/5Ni/7Mn/0.25C	65°C	mainly twinned	36
Fe/7Mn/0.25C	190°C	mainly twinned	36, 47
		for a given carbon level, manganese promotes twinning	
Fe/Ni/Ti		dislocations and twins depends on Ni/Ti & heat treatment	33
Fe/Cr/Ni Fe/Mn/Cr/Ni	metastable austenites	Low stacking fault energy dislocated α from ε	55, 56, 57, 21

TABLE I (cont.)

the habit plane must be actually {5, 10, 15}. In {259} martensites (bc tetragonal) there is one report of {110} as well as {112} twinned martensite plates (4, 49) (Fe-1.8%C steel).

It is likely that martensites in specimens prepared from bulk transformed alloys have undergone both transformation and accommodation deformation, so that it is not clear in cases where one finds both dislocated and twinned substructures, e.g. Fig. 5, which effect has dominated. Twins are found in lath martensites in several alloys (26, 54) (Fe/Ni/C, Fe/Ni/Co/C, Fe/Ni/Mn/C, Fe/Ni/Cr/C) and debate is occurring as to whether or not these twins are due to plastic deformation of the transformed martensite.[26]

3.2. Doubly Twinned Martensites

The twinned structures of martensites exhibiting $\{225\}_\gamma$ and $\{259\}_\gamma$ habits are particularly puzzling to the crystallographers, and there is no satisfactory explanation for these habits in terms of the observed structures and lattice invariant shears. However, until now it has not been shown that the twin structure is itself complex. The following results show that the twins themselves may be twinned.

The proof of this phenomenon requires painstaking experiments by electron microscopy and involves detailed dark field analyses of all the spots in the pattern. It is also helpful in the analysis to study orientations where martensite twins are parallel to the electron beam, e.g. $\langle 113 \rangle_\alpha$ foils, and plates in which the twins are inclined, e.g. $\langle 122 \rangle_\alpha$. These have been studied in Fe/33Ni and Fe/25Ni/0.3V/0.3C alloys. The results are shown in Figures 8-11.

Figure 9(c-f) shows a set of dark field images corresponding to the spots in Fig. 9(b) indexed in Fig. 10(c). If the $[22\bar{1}]$ martensite were

singly twinned on the $(11\bar{2})_\alpha$ the $[00\bar{1}]_\alpha$ twin orientation would be produced and the pattern would be superposed $[00\bar{1}]_\alpha$ and $[22\bar{1}]_\alpha$. If this were true, then dark field images of both 110_α and $1\bar{1}0_\alpha$ diffraction spots would reveal twin contrast. However, as the dark field images of Fig. 9c, d show, the twin reversal only occurs for one and not both of these reflections. The explanation is that the twins on $(11\bar{2})_\alpha$ are themselves twinned on $(\bar{1}12)_\alpha$ so that the $[00\bar{1}]_\alpha$ twin of $[22\bar{1}]_\alpha$ now transforms locally into the $[2\bar{2}\bar{1}]_\alpha$ orientation. However, the extent of the double twinning is limited. The contrast at S in Fig. 8 is consistent with secondary twins on $(11\bar{2})_\alpha$ in the primary twins. The dark field image of the spot marked "T" (Fig. 8c) reverses the contrast of both primary and secondary twins. This spot is actually the superposition of both $(110)_\alpha$ primary twin and $(\bar{1}\bar{1}0)_\alpha$ secondary twin reflections.

These conclusions regarding twinned twins are further confirmed by analysis of the edge-on twins in the fully twinned $[113]_\alpha$ martensite plate of Fig. 11. Here the primary twin plane is $(21\bar{1})_\alpha$ which produces the $[113]_\alpha \rightarrow [\bar{1}\bar{1}\bar{3}]_\alpha$ twinning transformation as verified by the diffraction pattern and dark field analysis. However, this example is even more complex. Faint streaks are resolvable on the negative of Fig. 11(b) parallel to the <110> directions indicated on this pattern. These streaks cannot be explained by double {112} twinning as in Figs. 8, 9, but they must be caused by planar defects on {110} e.g. twins although this is not expected in cubic martensite. However, since the diffraction streaks are so weak, it is not possible to resolve their morphological origin in the image. It is important to emphasize here that although Fe-Ni martensites are well characterized macroscopically, it is clear that there

are complications when each individual martensite crystal is analyzed. Differences can exist locally in composition and Ms temperature, and this could result in martensite plates of different habits and transformation substructures. The complexity of the situation is emphasized by the fact that Figs. 9 and 11 were obtained on the same specimen and within 10 microns of each other.

It is interesting to note that the interface in Fig. 11 is parallel to $(\bar{7}\bar{3}9)_\alpha$. Assuming a Bain correspondence this plane would be parallel to the $(\bar{5}29)$ of austenite. Although this is a speculative correlation at this stage, it is possible that $\{110\}_\alpha$ secondary twinning may be a characteristic of low temperature $(259)_\gamma$ habits. As more detailed analyses of martensite substructure are obtained, it is hoped that further clarification of the habits in terms of transformation shears will be possible.

It is noted that the twins are often displaced or truncated along $\langle 111\rangle_\alpha$, i.e. parallel to $\{011\}_\alpha$ traces consistent with slip (or possibly twin) deformation. Dislocations can be resolved between the twins in Fig. 5, but in general the contrast requirements are different for revealing twins and dislocations separately.

There is surface structure resolvable on the broad faces of the twins as can be seen in Fig. 1(d), Figs. 7 and 9. Some of the complex fringe patterns observed in the dark field images Fig. 9c-f may be related to the secondary twinning or to variations in twin thickness, e.g. at ledges. These fringes may also be associated with regular arrays of twin/twin or twin/matrix interface dislocations, but it has been difficult to obtain definitive images even after using several different

reflections, Fig. 9c-f. The fact that these fringes do not change orientation (direction) when different reflections are used (Fig. 9) rules out the possibility of Moiré contrast. Other separate experiments show that complex dislocation arrangements are present in addition to twinning. Figure 5 is an example. The dislocations shown here cannot be a/6<111> twinning dislocations since all are invisible in the g = [110] reflection (g.b = 1/3 or 0).

It may be argued that the double twinning may result from plastic deformation after transformation. However, the fact that double twins are observed in martensites formed directly in thin foils (Figs. 7, 8) lends good support for the belief that double twinning is characteristic of the transformation itself. Double twinning has also been detected in lath martensite, see ref. 26.

The absence of reports of double twinning in earlier electron microscopic studies of martensites is somewhat surprising, but serves to emphasize the necessity of doing complete dark field and diffraction analyses to characterize microstructure.

3.3. Factors Affecting Substructure

Recently Nutting[6] reviewed some of the factors thought to be important in controlling the martensite substructure, and in view of more recent data (Table 1) it is useful to summarize these factors so as to attempt to gain a comprehensive understanding. These factors are:

(1) Composition: Increasing the total solute content tends to change the morphology from dislocated laths to twinned plate martensite (Table 1). Carbon appears to have the strongest effect in promoting twinning.

(2) Ms temperature: Concurrently with composition there is usually a decrease in Ms temperature with increasing solute content: the exception is cobalt -- however, cobalt does not decrease twinning.[31,35] In a given alloy series the Ms can be kept constant and then the composition determines whether laths or plates form.[31]

(3) The strength of the martensite: Since the lattice invariant shear involves plastic deformation, the substructure must depend on the yield strength of martensite. This property also depends on composition and temperature. The strength of austenite and deformation substructure in austenite (e.g. Fig. 3) may also influence the morphology, but this possibility has not yet been studied in any detail.

(4) Austenite stacking fault energy: There is no simple relationship. High stacking fault energy (SFE) is supposed to promote laths if Ms is relatively high, but if Ms is low, twinned plates are formed.[6] However, increasing the concentration of all solutes seems to promote twinning, e.g. Mn and Ni, yet Mn lowers SFE and Ni raises SFE of austenite. It is difficult to see what relationship exists between stacking fault energy of austenite and transformation substructure of martensite unless the latter is influenced by the mode of plastic deformation of austenite during transformation. SFE of austenite is important, however, in determining whether ϵ martensite is preferred to α.[16,17,56,57]

(5) Cooling Rate: Cooling rate affects Ms,[28,54] and in lath martensites the dislocation density varies;[28] in alloy steels precipitation on slow cooling raises Ms so that the martensite is diluted and hence is lath type. Fast cooling retains solutes in solution and twinned

plates result.

(6) Thermal-mechanical: Plastic deformation can cause precipitation in austenite (ausforming),[29,30] so that on transformation lath martensite is formed. Likewise prior ausaging can affect the subsequent martensitic structure.[33]

(7) Transformation morphology is determined by pressure. In Fe-C alloys twinned plates can be produced at 40 kb whereas at atmospheric pressure, the martensite is lath type.[59,60]

All of these results lead to one consistent pattern, viz. the higher the solute content the greater is the probability of forming twinned plates. Conversely, if the austenite is diluted as a result of precipitation, e.g. by slow cooling, or by plastic deformation (ausforming) a normally twinned martensite can be changed to dislocated laths.[29,30] Results obtained recently on alloys with similar Ms temperatures and on the effects of cobalt clearly show that Ms temperautre alone is not the controling parameter determining the martensitic substructure.[31,35] These results have led to the suggestion[32] that the strength of martensite (and of the austenite from which it forms) is probably the single most important factor which determines whether martensite is dislocated or twinned or both.

This idea can be developed qualitatively by considering Fig. 12 which suggests schematically a variation in critical resolved shear stress with temperature for slip and twinning. This variation will depend on composition, and detailed knowledge of these relationships is needed. Increasing the solid solution composition and strength may raise the CRSS for slip above that for twinning so that twinning is the preferred shear mode. Similar relationships

might be expected for strain rate dependence. At low temperatures or when solutes lower CRSS for twinning, twinning is expected to be the preferred mode of plastic deformation. Also, since martensite forms over a range of temperature M_s-M_f [~ 100-200°C] and if this range includes the slip $\rightleftarrows$ twin transformation, then mixed substructures are expected. Likewise the local temperature rise at Ms and M_b could allow slip to occur when otherwise twinning dominates. It is also possible that different twinning or slip modes may operate at very low temperatures.

Carbon (and nitrogen) seems to be the most potent of the alloying elements in promoting twinning. Carbon is also the most potent strengthener of steel. Thus, the stronger the steel the more difficult it is for slip to occur and then twinning is preferred. This is also confirmed by the experiments of Richman[66] and Bevis et al.[67] who observed mechanical twins in deformed carbon martensites.

It may also be mentioned that the martensite substructure closely resembles that in shock-loaded materials.[24] In fcc metals as the shock pressure is increased twins are formed when the dislocation density has attained some critical value.[37,38] By analogy it is possible that the twins observed in martensite laths[31] may have been induced because the limiting dislocation density had already been attained. This would mean slip shears always precede twin shears.

Another factor which may be important is the driving force associated with the transformation. Bell and Owen[34] suggested that when a critical driving force is exceeded (~ 315 cal/mole) the change from dislocated to twinned martensite is expected. Pascover and Radcliffe[43] extended this concept to Fe/Ni and Fe/Cr where the driving force was in

the range 300-370 cal/mole for the Fe/29Ni alloy which is twinned. However, twins were not observed in their Fe/5Cr alloy although the driving force was 300-350 cal/mole. This can be explained on the basis that the CRSS for slip vs. that for twinning is the important parameters.

4. Diffraction Contrast

Whilst there are no real difficulties associated with distinguishing between the slip structure and twin structure within martensite, so far there have been very few quantitative analyses [see for example Patterscn and Wayman[41] and Warlimont[44]]. It is now clear that the twin structure itself is not simple. Although the twin planes can be characterized without too many difficulties, the twinning shear must be found by contrast analysis of the twinning dislocations. If the twins fully traverse the plate the dislocations terminate at the interface (γ-Ms or Ms-Ms) and the contrast analysis is then quite difficult. For {112} twins the Burgers vectors of the twinning dislocations are probably of the a/6 <111> type. For these to be observed, in general[7] $\vec{g}.\vec{b} > 1/3$, where $\vec{g}$ is the operating reflection. Thus a/6 <111> dislocations will not be visible with g = <110> nor <200>. Fringe contrast is observed only when $\vec{g}.\vec{R}$ is non-integral ($\vec{R}$ is the twin shear), i.e. when the phase shift $\alpha = 2\pi\vec{g}\vec{R}$ is non-zero (or $n2\pi$). For {112} <111>twinning in bcc metals, if $\vec{R}$ = 1/6<111> and since h + k + ℓ is always even, then α is $\pm 2\pi/3$ or zero and the contrast is identical to that for {111} <112> stacking faults in fcc crystals, as can be seen in Figs. 5, 8 (see also ref. 41). Hence the fringes are symmetrical in intensity in bright field and asymmetrical

in dark field. Thus, the suggestions of Krauss and Pitsch[53] regarding stacking faults in Fe/33%Ni can be explained in terms of thin twins although the argument could be more convincingly settled with respect to the evidence from the diffraction patterns (not available). Contrast analysis of {110} twinning has not yet been published. However, if the twinning displacement is also a/6<111> the fringe contrast from $\{112\}_\alpha$ and $\{110\}_\alpha$ martensitic twins would be identical since the fringe characteristics depend upon $\alpha = 2\pi \vec{g}.\vec{R}$. Thus, more detailed studies of the fringe character may be useful. Distinction between these different twin planes can in principle be obtained by trace analysis and from checks of the twinning reflections with the appropriate twinning rules [i.e. the twin reflection can be predicted from twinning analysis[10,51,52]]. The distinction is important with regard to the phenomenological theory of the transformation.

The above remarks on contrast apply, of course, to two-beam diffracting conditions and only for orientations when the matrix and twin diffraction vectors coincide. If the latter condition is not met, the fringe contrast will be modified due to the orientation difference across the matrix-twin interface (so-called excitation error, or ΔS fringes, e.g. Ref. 68). From a practical point of view and when examining commercial steels, it is virtually impossible to obtain two-beam orientations because of the small crystal size. This difficulty increases with increasing voltage, because of many beam excitations.

Except for Fe/Ni alloys the dislocated martensites are very complex and have not been analyzed, i.e. no determination of Burgers vectors have been made. In order for this to be done effectively, experiments

should involve pre-oriented single crystals and where transformation is incomplete so that constraints due to impinging martensite crystals can be avoided. In Fe/Ni alloys the dislocation structure[41,44] is often simple with long arrays of screws lying in <111>. However, in fully transformed steels the structure is far more complex and difficult to analyze (e.g. Fig. 6).

Transformation dislocations must remain with the interface and will not necessarily have simple Burgers vectors, i.e. a dislocation in austenite cannot of itself produce a martensitic structure unless it decomposes into partials which can accomplish the transformation. The simplest example of this is in fcc⇄hcp transformations which can be accomplished by splitting of the $1/2\langle 110\rangle_{fcc}$ dislocations into $1/6\langle 112\rangle$ or $1/3\langle 111\rangle$ partials, thus producing stacking faults and the hcp structure. Furthermore, if the habit plane is (111), successive shears by partials $1/6[\bar{2}11]$, $1/6[1\bar{2}1]$, $1/6[11\bar{2}]$ produce net zero shape change. Although the question of similar dissociations have been considered with respect to BCC → {FCC, HCP} transformations[50], specific attempts to identify the transformation dislocations, including a detailed study of the γ/Ms interface contrast, do not appear to have been published so far.

In studying the substructure of partially transformed alloys the substructures and interfaces of both phases will not generally be in contrast simultaneously. In order to resolve the relationship between the interface structure and the martensite substructure, it will be necessary to orient the foil for a strong martensitic reflection. Examples of the two contrast conditions are shown in Fig. 1 (ref. 20). Figure 1(a) is oriented for

martensite contrast and it is clear the martensite is made up of closely parallel BCC (twinned) blocks. In (b) which is oriented for austenite contrast the dislocation and faulted austenitic structure can be seen. Comparison of a and b shows that the dislocations are associated with the austenite phase. In (c) both are in contrast simultaneously.

It would be advantageous in such circumstances (i.e. overlapping phases) to do stereomicroscopy. In fact, greater use of this technique would be valuable.

5. Summary and Conclusions

It is clear that of the various physical features of martensitic transformations, two main areas are in need of elucidation, viz. nucleation, and detailed characterization of the transformation substructure and its relation to the transformation mechanism and crystallographic theory. Both of these problems are potentially solvable by direct studies of the transformation in the electron microscope. However, the fact remains that there are no conclusive results yet showing the nucleation site itself. Also, since the nucleation theory is unsatisfactory in its present form, the design of critical experiments to focus on these problems has been limited.

It is usually assumed that each martensite plate comes from one embryo. However, it is possible to have simultaneous nucleation of many embryos, which grow together to form plates. In other words there may not be a simple relationship between the number of nuclei and the number of martensite crystals. Direct observations are obviously necessary, and it will be useful to devote more time to experiments using high voltage electron microscopy in order to take advantage of the increased probability of

finding embryos, if they exist. Due to the increase in penetration the probability is an order of magnitude higher at 650 kV than at 100 kV. So far no attempt has been made in this direction except for copper alloys,[11] and these experiments were not related to the nucleation problem.

Questions can be raised regarding the value of thin foil observations for the interpretation of bulk transformations, and it is essential to compare foils with bulk materials. Nevertheless, useful information can be obtained and we have encouraging results that show at least substructural similarities, viz. double twinning in martensites formed in foils and in bulk specimens of the same alloy. It should be noted that whilst high voltage microscopy permits examination of thicker specimens, the upper useful limit of thickness for steels is still only of order 2μ at 500 kV-1000 kV, and this thickness is hardly representative of the bulk.

High voltage microscopy offers other advantages besides that of greater penetration. These advantages include the improvements in resolution due to decreased chromatic aberration, the great reduction in the minimum selected area of diffraction, the ability to examine the same area for extensive times without contamination being a limitation (the contamination rate is lowered by increasing electron energy, and the vacuum in high voltage microscopes is ~ 100 times better than at 100 kV), and the advantages of working with foils having large transparent areas available for analysis (e.g. Figs. 7, 9, 11). It should be noted, however, that radiation damage is a complicating factor at high voltages. Iron will suffer primary knock-on damage in electron

microscopes operated above 500 kV.

It has been suggested earlier and substantiated here that the strength and deformation characteristics of martensite (and possibly austenite) control the martensite substructure. In all cases the substructure is complex and probably involves several shear modes. There is a need for detailed data on the critical resolved shear stress dependence for slip and twinning as a function of composition, strain rate and temperature, before these suggestions can be properly evaluated.

Finally it can be said that apart from the considerable attention which has been paid to crystallographic relationships and the structure-properties approach, electron microscopy studies of martensite have, except in rare cases, neglected detailed contrast and diffraction analyses. Admittedly many martensites, particularly those in commercial steels, are far too complex for this to be facilitated. However, experimental alloys can be made so that partially transformed steels are available whereby crystallography, morphology and substructure can all be analyzed rigorously. If the same attention to detail, as far as electron metallography is concerned, is paid to ferrous martensites as has been paid to non-ferrous phase transformations we can look forward to a more complete understanding of this fascinating and important subject.

Acknowledgements

It is with great pleasure that I acknowledge the stimuli and help provided by past and present graduate students, particularly I. Cheng, S. Das, P. R. Okamoto, G. Stone, and M. Raghavan. I wish to thank the U.S.A.E.C. for continued financial support and Mr. D. Jurica for continued attention to the high performance of our 650 kV electron microscope.

Figure Captions

Fig. 1(a-d) Fe/8Cr/1C bulk transformed showing structure of austenite and martensite associated with twinned $(225)_\gamma$ plates. The primary $(112)_\alpha$ twins do not extend all across the larger plate in (d). Courtesy C. M. Wayman (ref. 20).

Fig. 2. Lath martensite in Fe/11.3Ni/7.5Co/0.24C/0.44Cr/0.3/Mn (Ms - 307°C). Laths occur as bundles of complex dislocated regions slightly misoriented from region to region. The diffraction pattern in (c) shows superposed $[100]_\alpha$ and $[111]_\alpha$ patterns which are a common feature. The regions corresponding to their orientations are revealed in the dark field images of spots A, B (ref. 31).

Fig. 3. Fe/25Ni/0.3V/0.3C Bulk transformed in liquid nitrogen. The lens shaped plate with $(112)_\alpha'$ twinned mid rib coexists with dislocated γ and untransformed γ. Notice the dense dislocation tangles, i.e. work hardened appearance in the austenite.

Fig. 4. Fe/33Ni/.01C Bulk transformed by quenching rapidly to liquid helium via iced brine and liquid nitrogen. Mostly twinned plates and retained austenite. The large plate (top left) is also heavily dislocated. 650 kV.

Fig. 5. Fe/33Ni/.01C As Fig. 4, same specimen, dark field image of matrix 110 spot showing twin fringe contrast as well as dislocations in two adjacent plates. 650 kV.

Fig. 6. Fe/28Ni/0.3C (Ms $\simeq$ 8°C) Bulk transformed in liquid nitrogen showing mixed complex structure of twinned and dislocated martensite. [Courtesy O. Johari].

Fig. 7. Fe/25Ni/0.3V/0.3C Thin foil transformed in liquid nitrogen showing partial twinning (compare to the same alloy, Fig. 3). The primary twins and fringe contrast are reversed in this dark field image of the 110_α twin spot. The twins are truncated parallel to $(110)_\alpha$ matrix. The broad faces of the twins contain structural details (cf. Fig. 1d) which may be ledges, secondary twins, or interface dislocations (see also Fig. 9). Orientation near $[3, 1, 11]_\alpha$. 650 kV.

Fig. 8. Fe/25Ni/0.3V/0.3C Thin foil transformed in the cold stage at -80°C showing the development of the doubly twinned substructure. The twin fringe contrast is strong near the extinction contour. The dark field image in (b) corresponds to position C in Fig. 10(c). Notice fine twin fragments, arrowed, and secondary contrast at S (consistent with secondary twin trace). This result proves that the twins are twinned.

Fig. 9. Fe/33Ni/.01C As Fig. 4, showing dark field experiments to reveal twinned {112} twins.

A. Bright field image.

B. Selected area diffraction of central part of A (see Fig. 10).

C. Dark field image of spot C $(110)T_1 + (\bar{1}\bar{1}0)T_2$. The twins show wedge fringe contrast at W.

D. Dark field image of spot D $(1\bar{1}0)$ matrix + $(\bar{1}10)T_1$.

E. Dark field image of spot E which is 200 T_1, or doubly diffracted matrix and T_2 spots.

F. Dark field image of $(\bar{2}\bar{4}0)T_1$ + (024) matrix.

In C the strong fringe contrast is due to wedge thickness changes.

The other fringes are parallel to the trace of $(\bar{1}12)$ in the $(00\bar{1})T_1$, and could represent double twin interface. 650 kV.

Fig. 10. Explanation of Fig. 9.

a) The pattern if the $22\bar{1}_\alpha$ matrix is singly twinned on $(11\bar{2})$; superposed $[22\bar{1}]_\alpha$ matrix + $(00\bar{1})_\alpha$ twin.

b) The pattern if the matrix is completely converted to the double twin $[00\bar{1}]T_1$ + $[2\bar{2}\bar{1}]T_2$.

c) The pattern if the $[22\bar{1}]_\alpha$ matrix twins to $[00\bar{1}]_\alpha$ and the $[00\bar{1}]_\alpha$ partially twins to $[2\bar{2}\bar{1}]_\alpha$. This pattern explains Fig. 9b upon analysis of the dark field images and comparison to the possibilities shown here, proving that the structure of Fig. 9 cannot be a single twin.

Fig. 11. Fe/33Ni/.01C Bulk transformed $[113]_\alpha$ orientation.

A. Bright field.

B. Selected area diffraction pattern showing strong streaks due to $(\bar{1}\bar{2}1)_\alpha$ primary twinning; double diffraction spots (white arrows) and very faint streaks along $\bar{1}10$ matrix and $\bar{1}10$ twin. $[\bar{1}\bar{1}3]_\alpha$ primary twin spot pattern is superposed on $[113]_\alpha$ matrix.

C. Dark field image of $\bar{1}10$ T_1 spot (which also includes the faint $\bar{1}10$ streaks).

D. Dark field image of $1\bar{1}0$ matrix. 650 kV.

Fig. 12. Schematic suggested variation of the stress for slip and twinning as a function of temperature. Composition variations are expected to affect the twin-slip cross-over and possible changes are indicated by arrows. The slip or twin modes may also vary with temperature and composition.

1. P. M. Kelly and J. Nutting, Proc. Roy. Soc., 1960, vol. 259A, p. 45.

2. P. M. Kelly and J. Nutting, JISI, 1959, vol. 192, p. 246; 1961, vol. 197, p. 199.

3. W. Pitsch, J. Inst. Metals, 1958, vol. 87, p. 444; Phil. Mag., 1959, vol. 4, p. 577.

4. C. M. Wayman: Recent Developments in Diffraction Methods in Mat. Sci. Proc. NATO Int. Summer School, Antwerp, Belgium, p. 187, North-Holland Publ., The Netherlands, 1970.

5. C. L. Magee: Phase Transformations, p. 115, ASM, Metals Park, Ohio, 1970.

6. J. Nutting, JISI, 1969, vol. 6, p. 872.

7. G. Thomas, Transmission Electron Microscopy of Metals, Wiley, New York, 1962; also Thin Films, ASM, 1964, p. 227.

8. G. Thomas, Trans. AIME, 1965, vol. 233, p. 1608.

9. G. Thomas, Recent Developments in Diffraction Methods in Mat. Sci. Proc. NATO Int. Summer School, Antwerp, Belgium, p. 131, North-Holland Publ., The Netherlands, 1970.

10. P. B. Hirsch, A. Howie, R. B. Nicholson, D. W. Pashley and M. J. Whelan: Electron Microscopy of Thin Crystals, Butterworths, London, 1965.

11. H. Fujita, Y. Kawasaki, E. Furubayashi, S. Kajiwara and T. Taska, Jap. J. Appl. Phys. 1967, vol. 6, p. 214.

12. G. Thomas, Phil. Mag., 1968, vol. 17, p. 1097.

13. E. Votava, Acta Met., 1960, vol. 8, p. 901; J. Inst. Met., 1961, vol. 90, p. 129.

14. J. A. Hren and G. Thomas, Trans. AIME, 1963, vol. 227, p. 308.

15. G. Thomas and M. J. Whelan, Phil. Mag., 1961, vol. 6, p. 1103.

16. P. L. Mangonon, Jr. and G. Thomas, Met. Trans., 1970, vol. 1, p. 1577.

17. J. A. Venables, Phil. Mag., 1962, vol. 7, p. 35.

18. S. R. Pati and M. Cohen, Acta Met., 1969, vol. 17, p. 189.

19. H. Warlimont, Trans. AIME, to be published.

20. K. Shimizu, M. Oka and C. M. Wayman, Acta Met, 1970, vol. 18, p. 1025.

21. G. Thomas: High Temperature, High Resolution Metallography (AIME), p. 217, Gordon and Breach, New York, 1967.

22. K. E. Easterling and P. R. Swann, Inst. Metals Mon. 33, 1969, p. 152.

23. K. Kinsman, 1970 EMSA Conference, Houston, p. 520, Claitors Publishers, New Orleans, La., 1970.

24. W. C. Leslie, D. W. Stevens and M. Cohen, High Strength Materials, p. 382, J. Wiley, New York, 1965.

25. K. Shimizu and C. M. Wayman, Acta Met., 1966, vol. 14, p. 1390.

26. S. K. Das and G. Thomas, Met. Trans. AIME, 1970, vol. 1, pp. 325, 2009.

27. P. M. Kelly, "Met. Developments in High Alloy Steels," British Iron and Steel Inst. special report, 1964, vol. 86, p. 146.

28. G. R. Speich and H. Warlimont, JISI, 1968, vol. 206, p. 385.

29. G. Thomas, D. Schmatz and W. W. Gerberich, High Strength Materials, p. 251, J. Wiley, New York, 1965.

30. O. Johari and G. Thomas, Trans. ASM, 1965, vol. 58, p. 563.

31. S. K. Das and G. Thomas, Trans. ASM, 1969, vol. 62, p. 659.

32. O. Johari and G. Thomas, Acta Met., 1965, vol. 13, p. 1211.

33. I-lin Cheng, Ph. D. Thesis, University of California, Berkeley, UCRL-19196.

34. T. Bell and W. S. Owen, Trans. AIME, 1967, vol. 239, p. 1940.

35. M. Raghavan, M. S. Thesis, University of California, Berkeley, UCRL-19132.

36. D. Huang and G. Thomas, Met. Trans. 1971, in press (UCRL-19692.

37. R. L. Nolder and G. Thomas, Acta Met. 1964, vol. 12, p. 227.

38. O. Johari and G. Thomas, Acta Met., 1964, vol. 12, p. 1153.

39. M. H. Richmon and M. Cohen, Mat. Sci. and Eng., 1968/9, vol. 3, p. 240.

40. A. R. Marder and G. Krauss, Trans. ASM, 1967, vol. 60, p. 651.

41. R. L. Patterson and C. M. Wayman, Acta Met., 1966, vol. 14, p. 347; See also 1964, vol. 12, p. 1306.

42. G. R. Speich and P. R. Swann, JISI, 1965, vol. 203, p. 480.

43. J. S. Pascover and S. V. Radcliffe, Trans. AIME, 1968, vol. 242, p. 673.

44. H. Warlimont, Electron Microscopy, p.HH6, Academic Press, New York, 1962.

45. K. Shimizu, J. Phys. Soc., Japan, 1962, vol. 17, p. 508.

46. J. W. Christian, Military Transformations ISI Spec. Rep. 93, 1965, p. 1.

47. T. Boniszewski, discussion of ref. 46, p. 20.

48. Z. Nishiyama and K. Shiwizu, Acta Met., 1961, vol. 9, p. 980.

49. M. Oka and M. Wayman, Trans. AIME, 1968, vol. 242, p. 337.

50. J. B. Cohen, R. Hinton, K. Lay and S. Sass, Acta Met., 1962, vol. 10, p. 894.

51. O. Johari and G. Thomas, Stereographic Projection and its Applications, Interscience, New York, 1969.

52. R. Bullough and C. M. Wayman, Trans. AIME, 1966, vol. 236, p. 1704.

53. G. Krauss and W. Pitsch, Trans. AIME, 1965, vol. 233, p. 919.

54. G. S. Ansell, V. I. Lizunov, and R. W. Messler, Trans. J.I.M. Suppl. 9, 1968, p. 933.

55. W. S. Owen, E. A. Wilson and T. Bell, High Strength Materials, p. 167, J. Wiley, New York, 1965.

56. P. M. Kelly, Acta Met., 1965, vol. 13, p. 635.

57. J. F. Breedis, Acta Met., 1965, vol. 13, p. 239.

58. J. K. Abraham and J. S. Pascover, Trans. AIME, 1969, vol. 245, p. 759.

59. S. V. Radcliffe and M. Schatz, Acta Met., 1962, vol. 10, p. 201.

60. R. F. Vyhnal and S. V. Radcliffe, Acta Met., 1967, vol. 15, p. 1475.

61. J. M. Chilton, C. J. Barton and G. R. Speich, JISI, 1970, vol. 208, p. 184.

62. P. C. Rowlands, E. O. Fearon and M. Bevis, Inst. Metals Mon. 33, 1969, p. 194.

63. D. S. Lieberman, Acta Met., 1966, vol. 14, p. 1723.

64. A. F. Acton and M. Bevis, Mat. Sci. and Eng., 1969, vol. 5, p. 19.

65. N. D. H. Ross and A. G. Crocker, Acta Met., 1970, vol. 18, p. 405.

66. R. H. Richman, Trans. AIME, 1963, vol. 227, p. 159.

67. M. Bevis, P. C. Rowlands and A. F. Acton, Trans. AIME, 1968, vol. 242, pp. 1555, 1559.

68. R. Gevers, P. Delavignette, H. Blank, J. van Landuyt and S. Amelinckx, phys. stat. sol., 1964, vol. 4, p. 383.

69. G. Thomas, I-lin Cheng, and J. R. Mihalisin, Trans. ASM, 1969, vol. 62, p. 852.

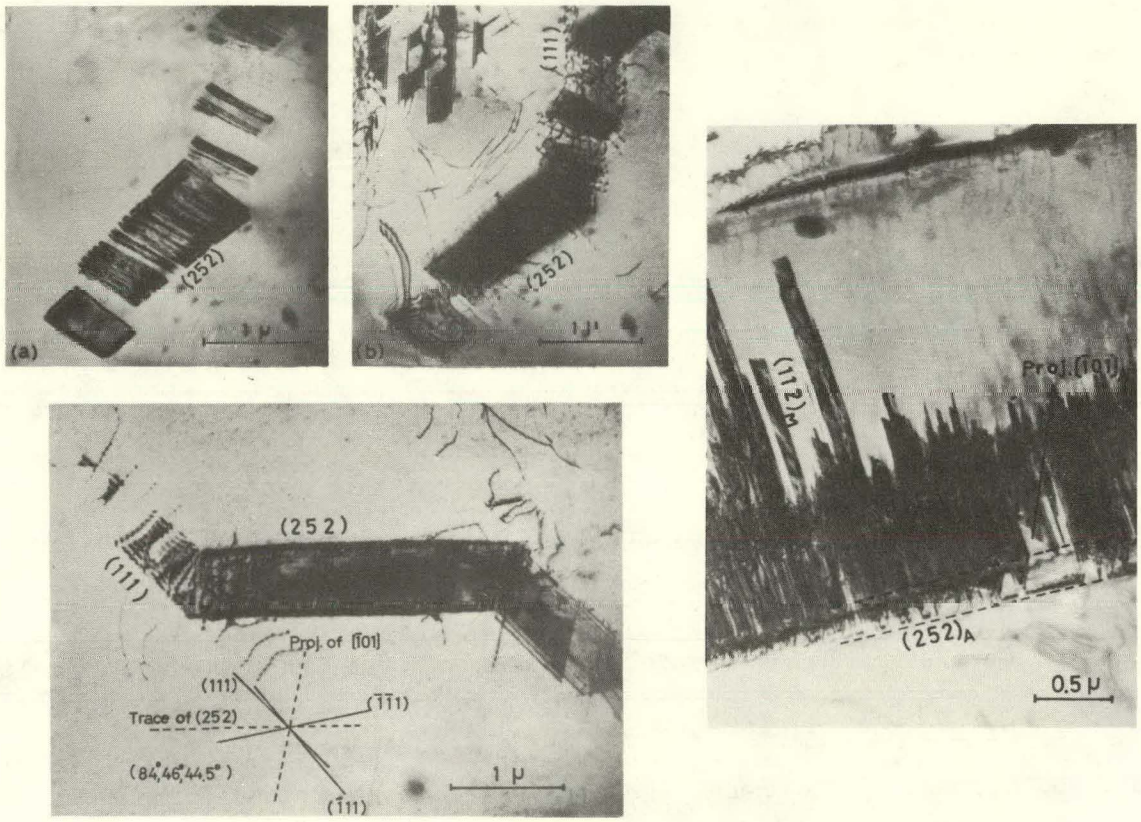

XBB704-1963

Fig. 1.

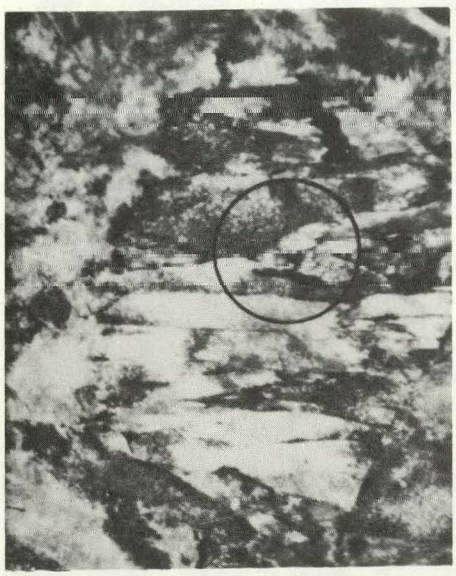

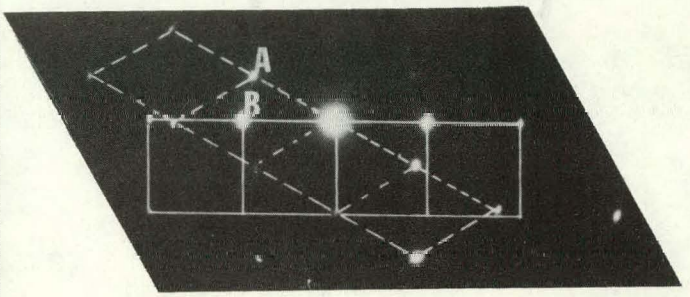

—— [1 0 0]

- - - - [1 1 1]

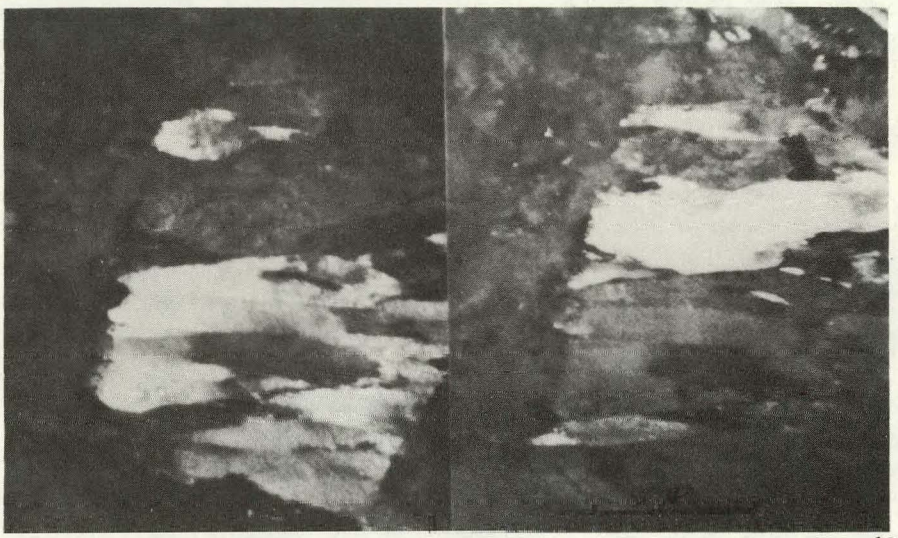

XBB6811-6972-A

Fig. 2.

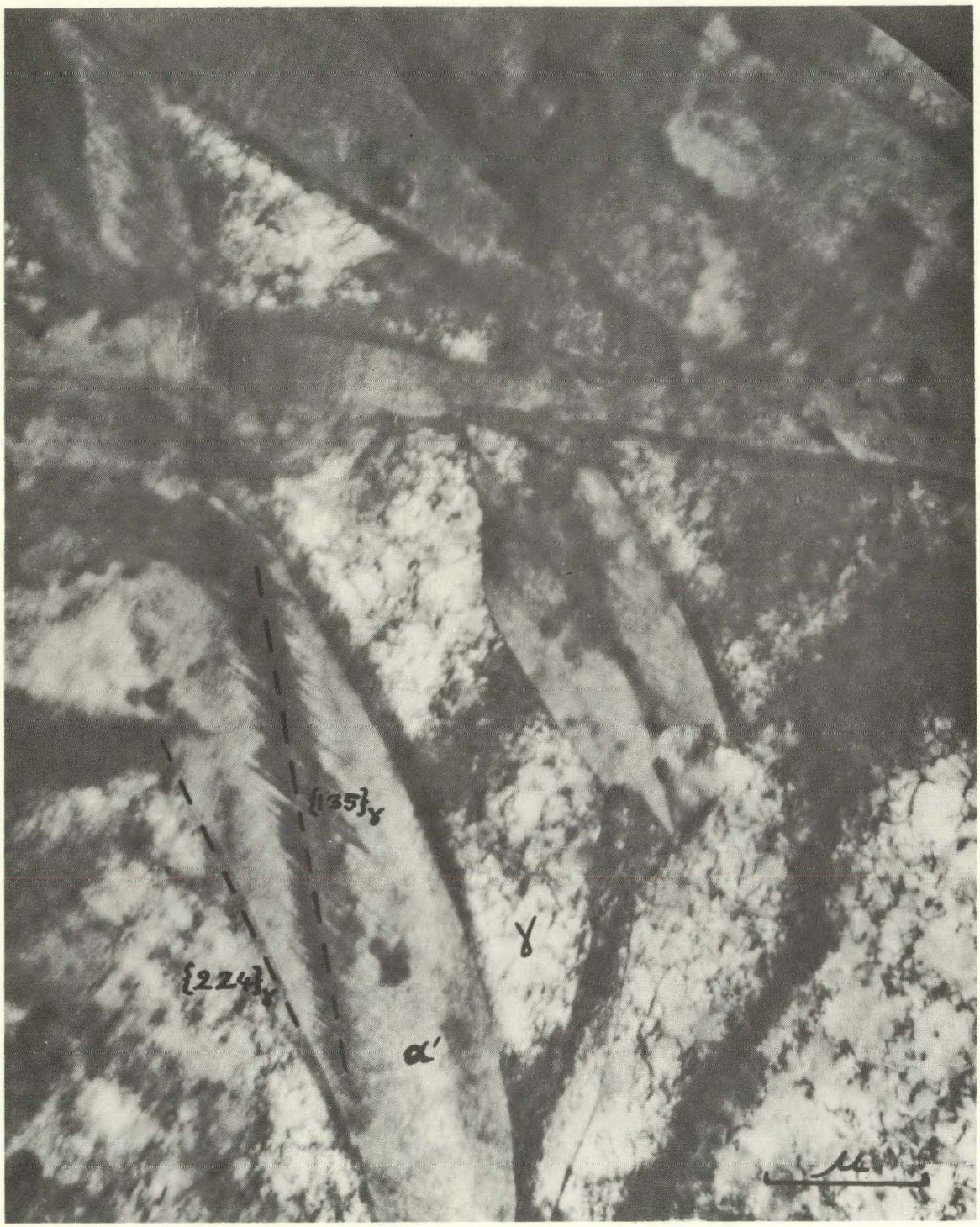

XBB7010-4439

Fig. 3.

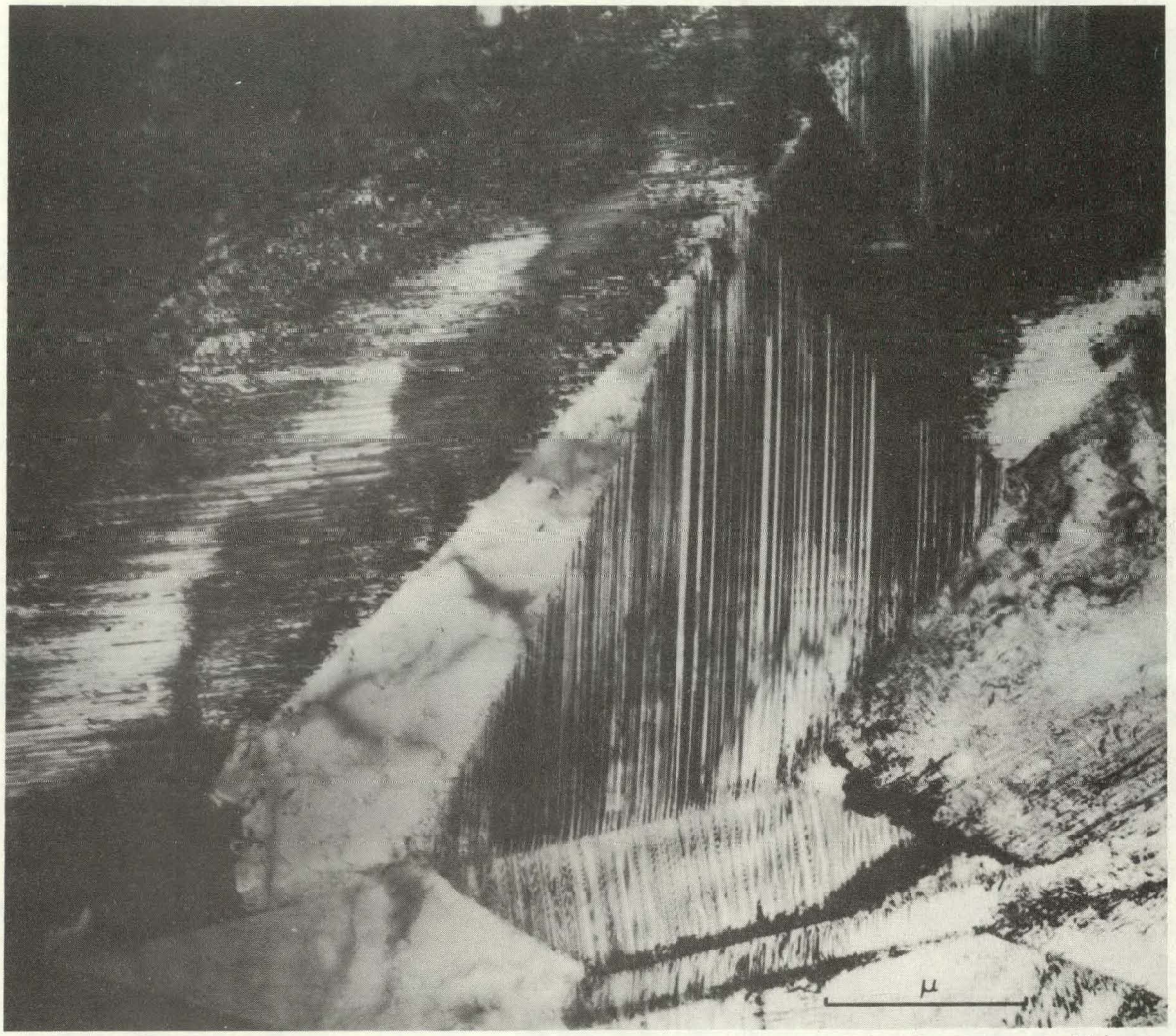

XBB7010-4440

Fig. 4.

XBB7010-4371

Fig. 5.

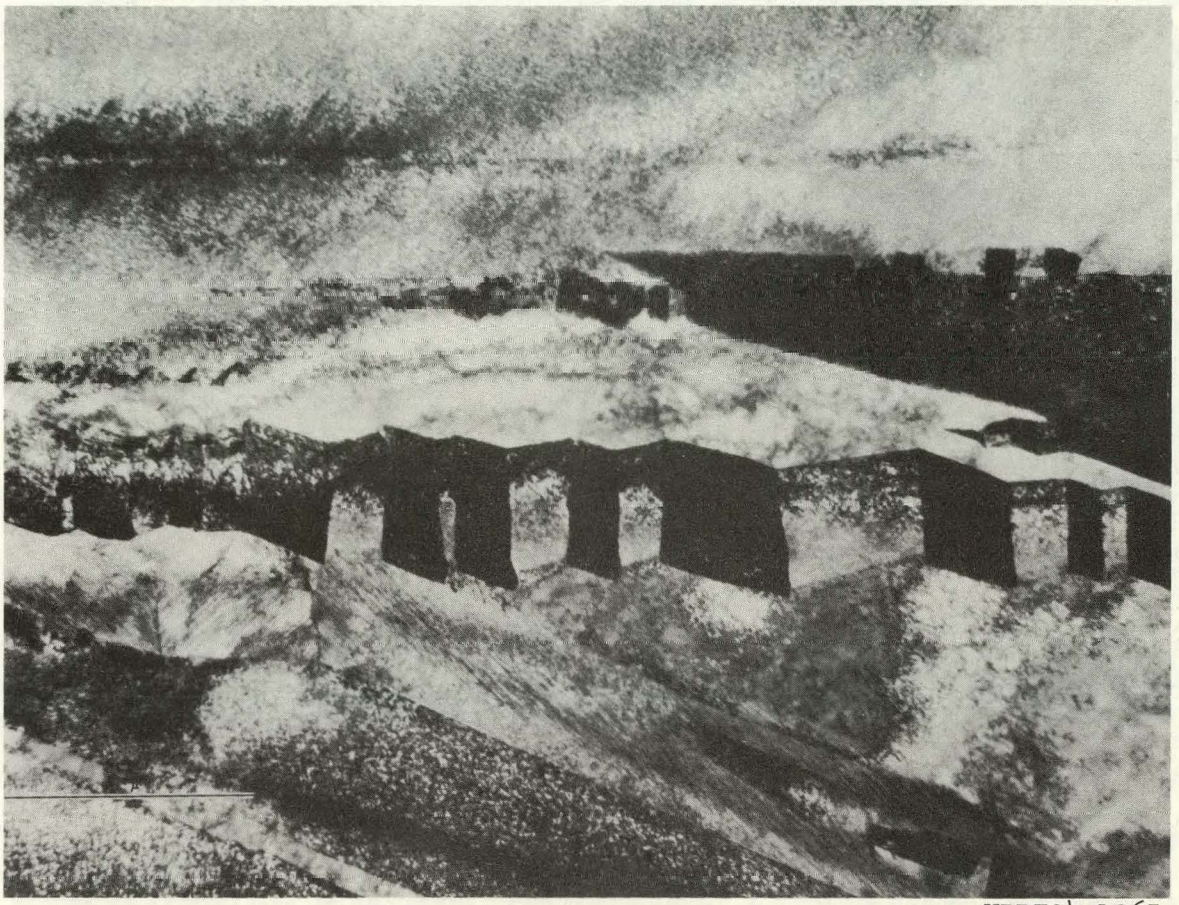

XBB704-1965

Fig. 6.

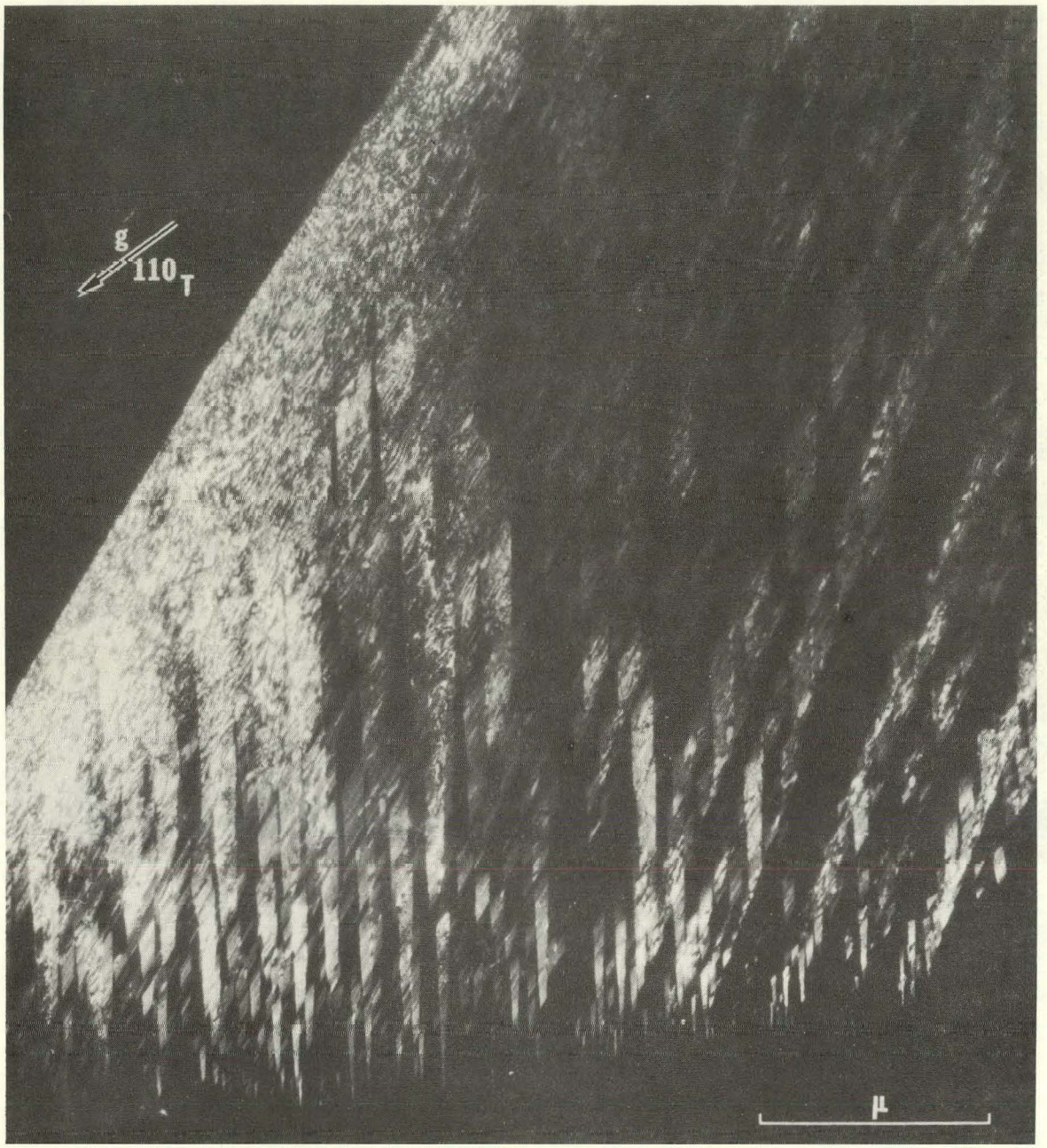

XBB7010-4374

Fig. 7.

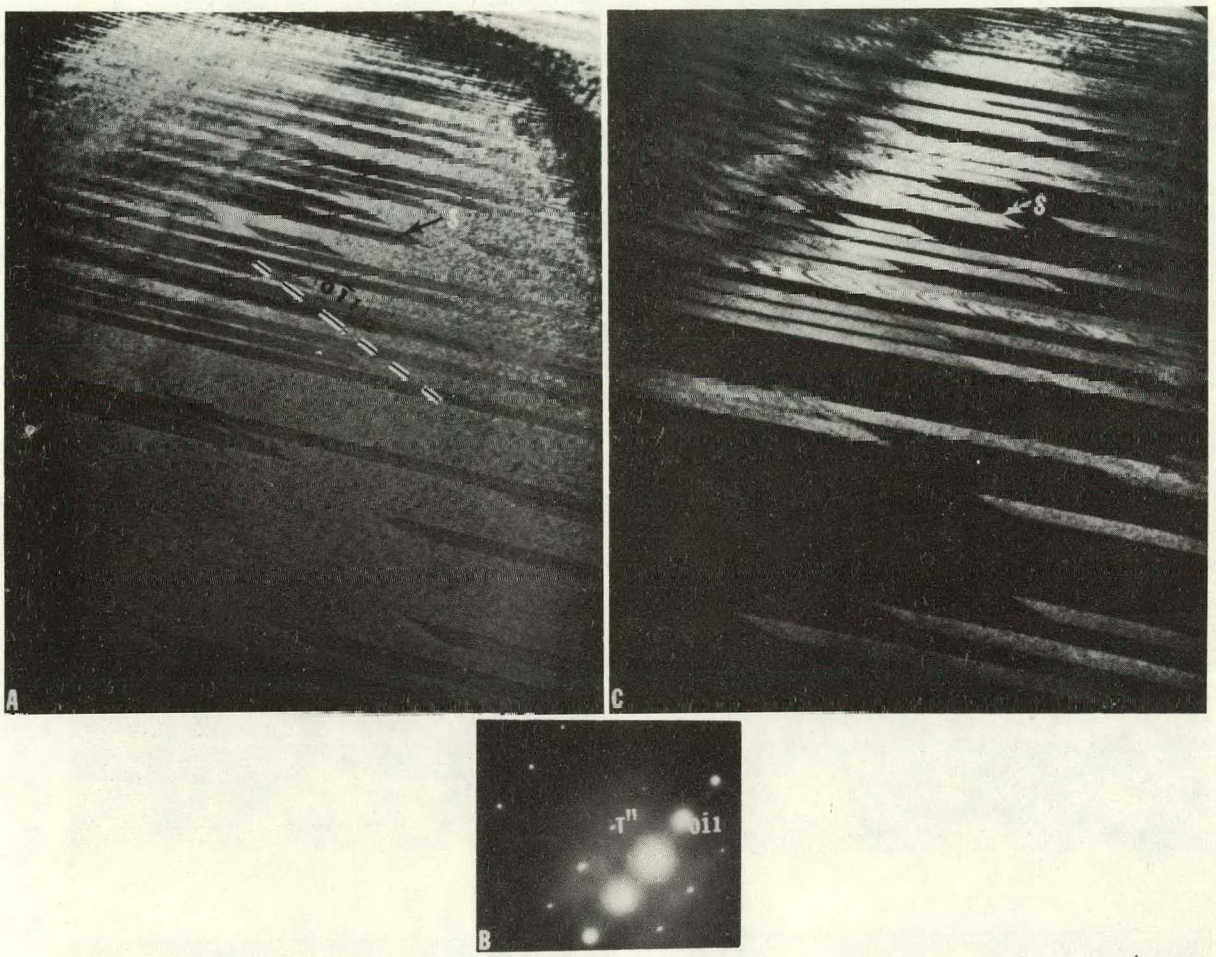

XBB7010-4372

Fig. 8.

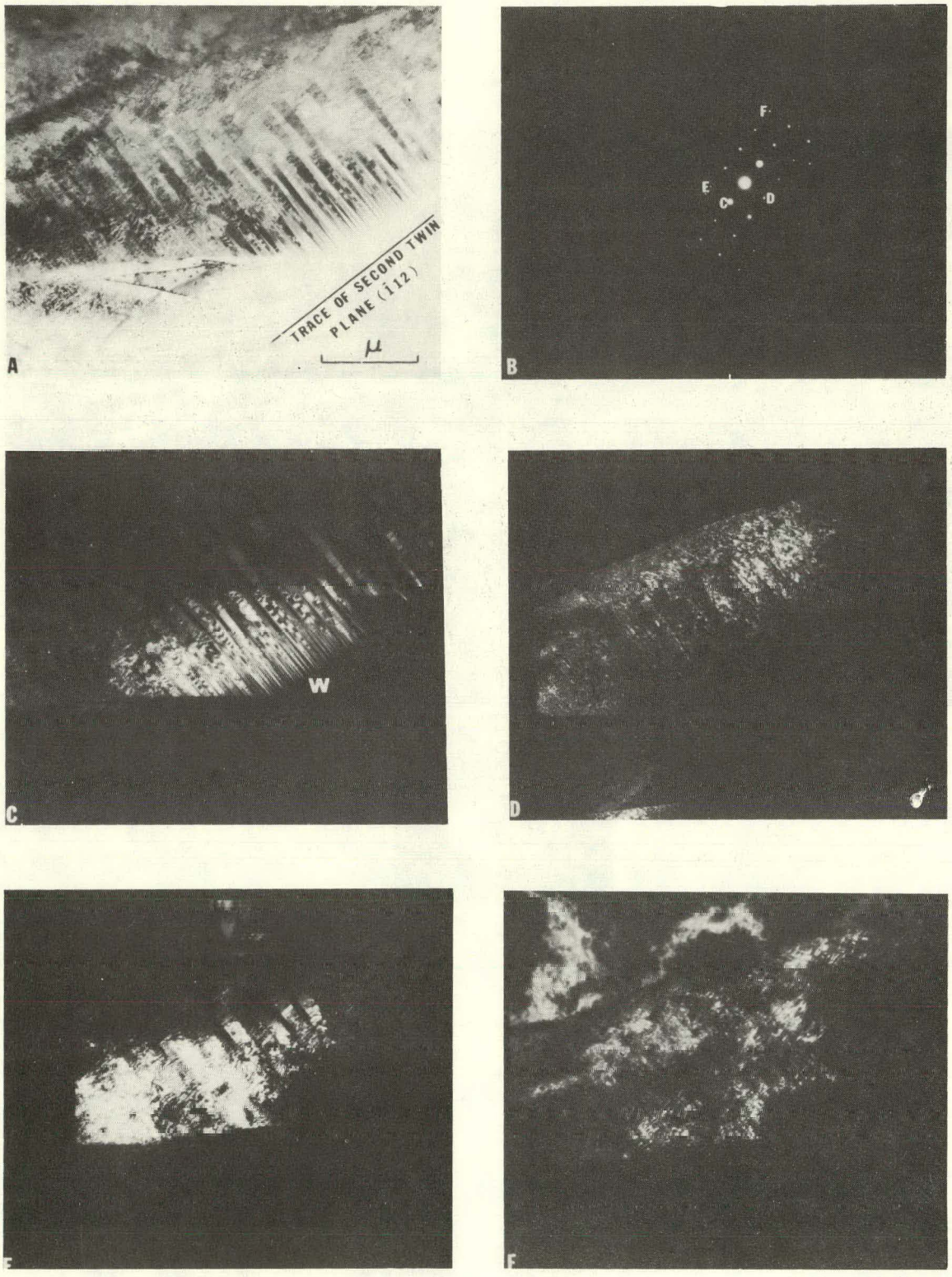

XBB7010-4373

Fig. 9.

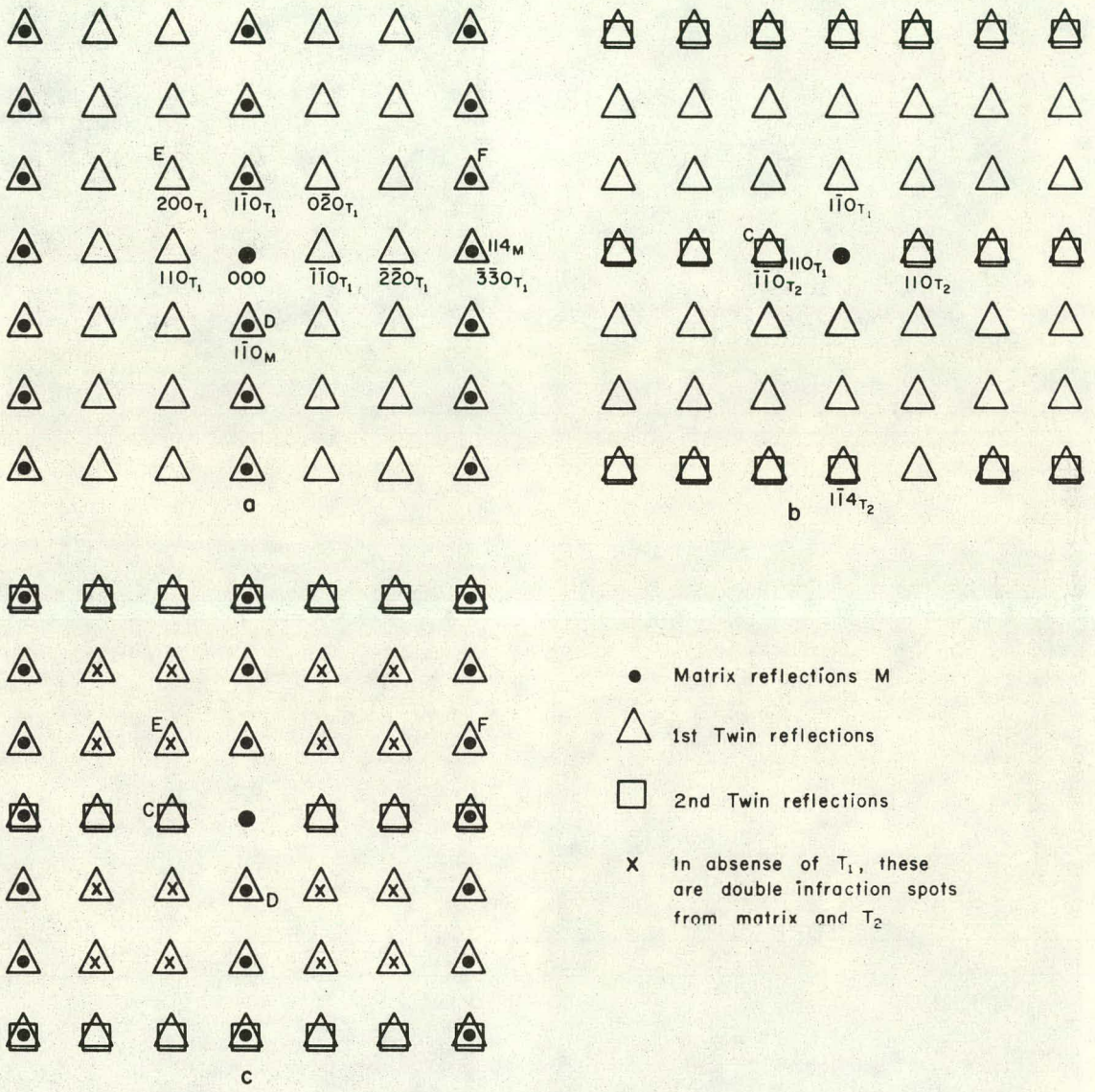

XBL706-3131

Fig. 10.

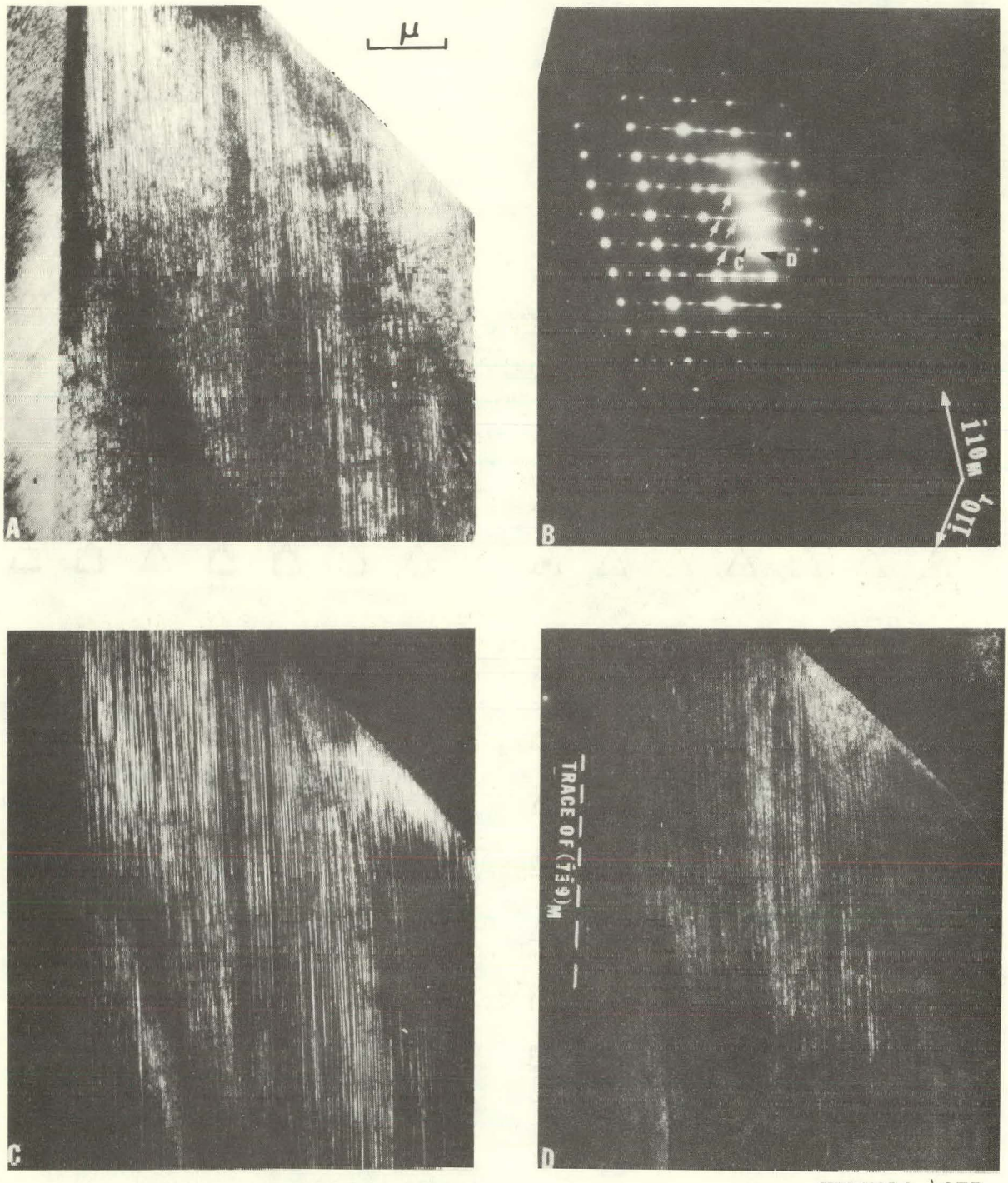

XBB7010-4375

Fig. 11.

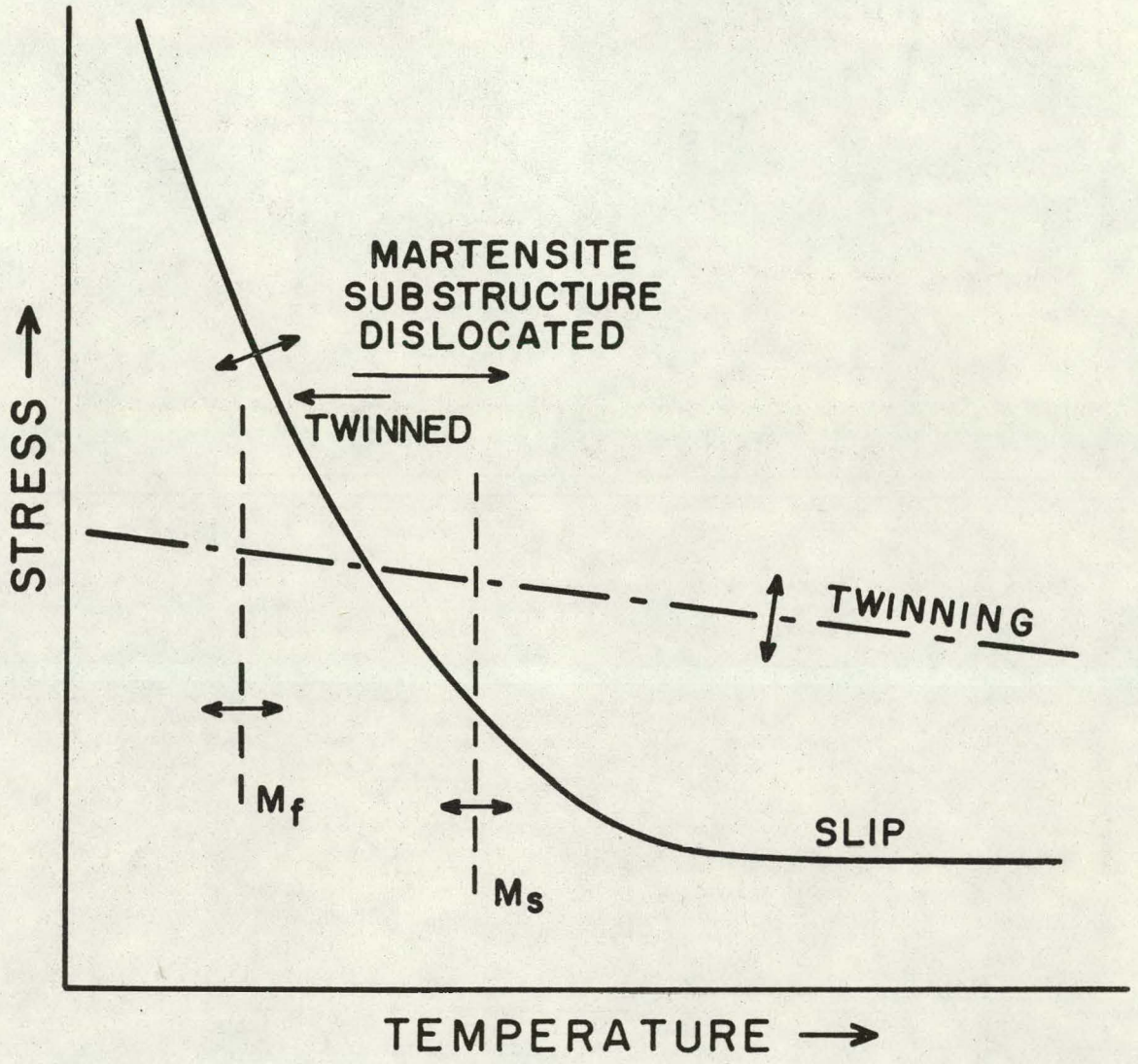

XBL 705-890

Fig. 12.

TECHNICAL INFORMATION DIVISION
LAWRENCE RADIATION LABORATORY
UNIVERSITY OF CALIFORNIA
BERKELEY, CALIFORNIA 94720